Activationless generation-recombination current in semimetallic heterostructures: application to InAs/GaSb

1998 J. Phys.: Condens. Matter 10 4257

(http://iopscience.iop.org/0953-8984/10/19/013)

J. Phys.: Condens. Matter **10** (1998) 4257–4266. Printed in the UK PII: S0953-8984(98)87893-4

Activationless generation–recombination current in semimetallic heterostructures: application to InAs/GaSb

Wayne Lau and Mahi R Singh

Department of Physics and Astronomy, University of Western Ontario, London, Ontario, Canada N6A 3K7

Received 25 September 1997, in final form 30 January 1998

Abstract. A theory for the activationless generation–recombination current density in type II heterojunctions such as InAs/GaSb is developed on the basis of the 8×8 $\boldsymbol{k}\cdot\boldsymbol{p}$ matrix Hamiltonian (the Bodnar model). The activationless recombination rate and current–voltage characteristics of an InAs/GaSb heterojunction are calculated. It is found that under a forward bias the current density increases with increasing applied voltage, finally becoming non-linear. At small applied voltages, the current–voltage characteristics are linear and the heterojunction has the properties of an Ohmic contact. This is in agreement with the experimental results.

1. Introduction

There has been considerable interest in the study of InAs/GaSb type II heterostructures and superlattices using molecular-beam epitaxy techniques (Sakaki *et al* 1977, Kono and McCombe 1997). The transport and optical properties of these systems have been the subject of various experimental and theoretical investigations (Bastard 1988). InAs/GaSb superlattices exhibit an interesting semiconductor-to-semimetal transition (Sakaki *et al* 1977, Barnes *et al* 1993). Recently we found that the semiconductor-to-semimetal transition in InAs/GaSb superlattices depends not only on the layer thickness but also on the anisotropy of the band structure of the samples and the band overlap of the two constituent semiconductors (Lau and Singh 1996a, b).

In direct-gap semiconductors, an electron from the conduction band can make a transition down to the valence band and subsequently recombines with a hole via the emission of a photon. This process is called *direct recombination*. On the other hand, in the case of indirect-gap semiconductors, the emission of a photon due to the recombination of an electron and a hole usually involves the emission of a phonon to satisfy conservation of momentum. This process is called *indirect recombination*. It is important to note that both processes occur in the presence of a third particle such as a photon, phonon, or impurity. The aim of the present paper is to propose a theory for electron–hole recombination processes which do not require the presence of a third particle. These types of recombination process can occur in semimetallic type II heterostructures such as InAs/GaSb. In A/B type II heterostructures, the conduction band of the A semiconductor lies beneath the valence band of the B semiconductor. This negative, or crossed-gap configuration of A/B heterostructure leads to a charge transfer between the A and B semiconductors which generates intrinsic carriers (electrons and holes) on either side of the interface. Due to the band overlap between the conduction band of A and the valence band of B, there are activationless recombination

0953-8984/98/194257+10$19.50

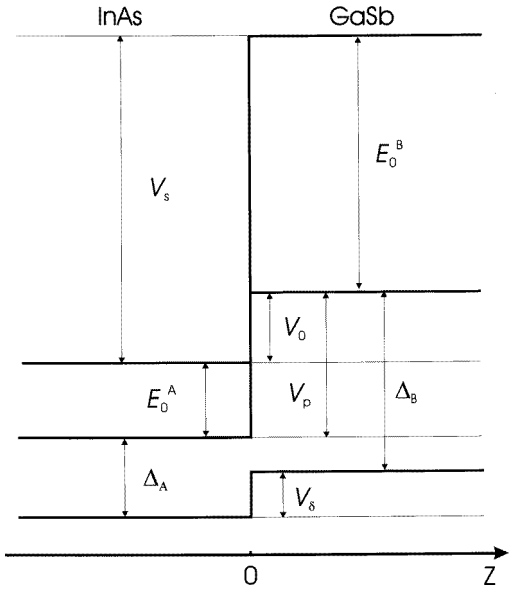

Figure 1. The potential band-edge profile of an InAs/GaSb heterojunction.

processes which do not require the presence of any third body. Therefore, we call this *activationless recombination.*

We have developed a theory for the current density due to the activationless generation–recombination processes in type II heterojunctions. Analytical expressions for the activationless generation rate, recombination rate, and current density were derived in the framework of the envelope function approximation based on the Bodnar model (Bodnar 1978). We numerically calculated the recombination rate, current–voltage characteristics, and conductance of an InAs/GaSb heterojunction. In addition, we also calculated the current density as a function of the temperature of the heterojunction. We found that under a forward bias the current density increases with increasing applied voltage, eventually becoming non-linear. We also found that the current–voltage characteristics are linear at a small voltage. This implies that the InAs/GaSb heterojunction has the properties of an Ohmic contact for low voltages, in agreement with the experimental results (Esaki 1980).

2. Theory

We consider the Bodnar 8×8 $\boldsymbol{k} \cdot \boldsymbol{p}$ matrix Hamiltonian (Bodnar 1978). This model includes the electron–hole interaction along with non-parabolicity and anisotropy of the band structure, whereas the Kane model does not include the latter effect (Bastard *et al* 1991, Seiler *et al* 1977). The Bodnar model has been extensively used by Singh and Wallace (Wallace 1979, Singh and Wallace 1983) and others (Lamrani and Aubin 1987) to calculate the optical and transport properties of narrow-gap semiconductors. The electronic structure of semiconductors such as InAs and GaSb can be described by a pseudoangular momentum $\boldsymbol{J}$ and its projection J_z along the z-axis. The Γ_6 symmetry corresponds to $(J, J_z) = (\frac{1}{2}, \pm\frac{1}{2})$, the Γ_8 symmetry corresponds to $(J, J_z) = (\frac{3}{2}, \pm\frac{3}{2})$ and $(J, J_z) = (\frac{3}{2}, \pm\frac{1}{2})$, and the Γ_7 symmetry corresponds to $(J, J_z) = (\frac{1}{2}, \pm\frac{1}{2})$. Furthermore, the $J_z = \pm\frac{3}{2}$ states

correspond to the heavy particles—Γ_8 heavy holes (HH), and the $J_z = \pm\frac{1}{2}$ states correspond to the light particles—Γ_6 electrons, Γ_8 light holes (LH), and Γ_7 spin–orbit split-off holes (Bastard *et al* 1991).

Here we consider an A/B semiconductor heterostructure which is grown along the z-axis and in which electrons are free to move in the X–Y plane. The potential profile of an InAs/GaSb semimetallic heterojunction is shown in figure 1. The potential steps $V_s(z)$, $V_p(z)$, and $V_\delta(z)$ shown in the figure arise from the band offsets of the conduction and valence band edges across an interface due to the mismatch of the band gaps at the interface. Here $V_s(z) = V_0 + E_0^A$ is the Γ_6 offset, $V_p(z) = V_0 + E_0^A$ is the Γ_8 offset, and $V_\delta(z) = V_0 + E_0^A + \Delta_A - \Delta_B$ is the Γ_7 offset, where V_0 is the band overlap, E_0^A and Δ_A respectively are the energy gap and the spin–orbit coupling parameters of the InAs semiconductor, and E_0^B and Δ_B respectively are the energy gap and the spin–orbit coupling parameters of the GaSb semiconductor. The energy zero is taken at the Γ_6 edge, which is the bottom of the bulk InAs conduction band. The potential can be written as $V_{s,p,\delta}(z) = V_{s,p,\delta}Y(z)$ where $Y(z) = 0$ for $z \leqslant 0$, and $Y(z) = 1$ for $z > 0$. Note that the zero of the z-axis is taken at the interface of the heterojunction. We modify the Bodnar Hamiltonian for type II heterostructures, and it is written as

$$\begin{bmatrix}
V_s(z) & 0 & E & \sqrt{\frac{2}{3}}P_\parallel k_z & -\sqrt{\frac{1}{3}}P_\perp k_+ & 0 & \sqrt{\frac{1}{3}}P_\parallel k_z & \sqrt{\frac{2}{3}}P_\perp k_+ \\
0 & V_s(z) & 0 & \sqrt{\frac{1}{3}}P_\perp k_- & \sqrt{\frac{2}{3}}P_\parallel k_z & D & -\sqrt{\frac{2}{3}}P_\perp k_- & \sqrt{\frac{1}{3}}P_\parallel k_z \\
D & 0 & A & 0 & 0 & 0 & 0 & 0 \\
\sqrt{\frac{2}{3}}P_\parallel k_z & \sqrt{\frac{1}{3}}P_\perp k_+ & 0 & B & 0 & 0 & -\sqrt{\frac{2}{9}}\delta & 0 \\
-\sqrt{\frac{1}{3}}P_\perp k_- & \sqrt{\frac{2}{3}}P_\parallel k_z & 0 & 0 & B & 0 & 0 & -\sqrt{\frac{2}{9}}\delta \\
0 & E & 0 & 0 & 0 & A & 0 & 0 \\
\sqrt{\frac{1}{3}}P_\parallel k_z & -\sqrt{\frac{2}{3}}P_\perp k_+ & 0 & -\sqrt{\frac{2}{9}}\delta & 0 & 0 & C & 0 \\
\sqrt{\frac{2}{3}}P_\perp k_- & \sqrt{\frac{1}{3}}P_\parallel k_z & 0 & 0 & -\sqrt{\frac{2}{9}}\delta & 0 & 0 & C
\end{bmatrix} \tag{1}$$

where the diagonal elements A, B, and C are

$$A = -E_0^A + V_p(z)$$
$$B = -E_0^A - \frac{2}{3}\delta + V_p(z)$$
$$C = -E_0^A - \Delta_A - \frac{1}{3}\delta + V_\delta(z)$$

and we have made the replacements

$$D = P_\perp k_+ \qquad E = P_\perp k_-$$

for reasons of space. Here $k_\pm = \sqrt{1/2}(k_x \pm \mathrm{i}k_y)$. k_x, k_y, and k_z are the components of the wavevector $\boldsymbol{k}$ along $\boldsymbol{a}$ [100], $\boldsymbol{b}$ [010], and $\boldsymbol{c}$ [001] respectively. $P_\parallel$ and $P_\perp$ which are taken to be the same in the two semiconductors are the non-zero matrix Kane elements, and δ is the crystal-field anisotropy parameter (Singh and Wallace 1983). In equation (1) we have set $\hbar = 1$, $c = 1$, $e = 1$, and $m_0 = 1$. The eight-component eigenvectors $(|\phi_1\rangle, \ldots, |\phi_8\rangle)$

of the above Hamiltonian within each layer of the heterostructure are written as

$$\begin{aligned}
|\phi_1\rangle &= g_0^{-1}(P_\perp k_-|\phi_3\rangle + \sqrt{2/3}P_\parallel k_z|\phi_5\rangle - \sqrt{1/3}P_\perp k_+|\phi_6\rangle + \sqrt{2/3}P_\parallel k_z|\phi_7\rangle \\
&\qquad + \sqrt{2/3}P_\perp k_+|\phi_8\rangle) \\
|\phi_2\rangle &= g_0^{-1}(\sqrt{1/3}P_\perp k_-|\phi_4\rangle + \sqrt{2/3}P_\parallel k_z|\phi_5\rangle + P_\perp k_+|\phi_6\rangle - \sqrt{2/3}P_\perp k_-|\phi_7\rangle \\
&\qquad + \sqrt{2/3}P_\parallel k_z|\phi_8\rangle) \\
|\phi_3\rangle &= g_1^{-1}P_\perp k_+|\phi_1\rangle \\
|\phi_6\rangle &= g_1^{-1}P_\perp k_-|\phi_2\rangle \\
|\phi_4\rangle &= (g_1 + 2\delta/3)^{-1}(-\sqrt{2/3}P_\perp k_-|\phi_1\rangle + \sqrt{2/3}P_\parallel k_z|\phi_2\rangle - \sqrt{2/3}\delta|\phi_8\rangle) \\
|\phi_5\rangle &= (g_1 + 2\delta/3)^{-1}(\sqrt{2/3}P_\parallel k_z|\phi_1\rangle + \sqrt{1/3}P_\perp k_-|\phi_2\rangle - \sqrt{2/3}\delta|\phi_7\rangle) \\
|\phi_7\rangle &= g_2^{-1}(\sqrt{1/3}P_\parallel k_z|\phi_1\rangle - \sqrt{2/3}P_\perp k_+|\phi_2\rangle - \sqrt{2}/3\delta|\phi_4\rangle) \\
|\phi_8\rangle &= g_2^{-1}(\sqrt{2/3}P_\perp k_-|\phi_1\rangle + \sqrt{1/3}P_\parallel k_z|\phi_2\rangle - \sqrt{2}/3\delta|\phi_5\rangle)
\end{aligned} \tag{2}$$

where $g_0 = E - V_s$, $g_1 = E + E_0^A - V_p$, and $g_2 = E + E_0^A + \Delta_A + \delta/3 - V_\delta$.

From equation (2), we get two coupled equations in $|\phi_1\rangle$ and $|\phi_2\rangle$ within each layer of the system:

$$\begin{bmatrix} h_{11} & h_{12} \\ h_{21} & h_{22} \end{bmatrix} \begin{bmatrix} |\phi_1\rangle \\ |\phi_2\rangle \end{bmatrix} = 0. \tag{3}$$

The matrix elements of the equation above are given by

$$h_{11} = P_\perp^2(k_- g_1^{-1} k_+ + k_+ g_1^{-1} k_- + k_+ D^{-1} g_5 k_- + k_- D^{-1} g_5 k_+)/2 + P_\parallel^2(k_z D^{-1} g_4 k_z) - g_0 \tag{4a}$$

$$h_{12} = \sqrt{2}P_\parallel P_\perp(k_- D^{-1} g_6 k_z - k_z D^{-1} g_6 k_-)/3 \tag{4b}$$

where

$$\begin{aligned}
&h_{11} = h_{22} && h_{12} = h_{21}^\dagger \\
&g_3 = E + E_0^A + \Delta_A - V_\delta && g_4 = E + E_0^A + 2\Delta_A/3 - 2V_\delta/3 - V_p/3 \\
&g_5 = E + E_0^A + \Delta_A/3 - V_\delta/3 - 2V_p/3 && g_6 = \Delta_A - V_\delta + V_p \\
&D = \gamma/g_0 g_1 && \gamma = g_0 g_1(g_1 g_2 + 2\delta g_3/3).
\end{aligned}$$

By requiring continuity of the wavefunctions and the probability current across the interface between the two layers, we obtain the boundary conditions given by Lau and Singh (1996a, b). Using these boundary conditions, we calculate the reflected amplitude (C_r) and transmitted amplitude (C_t) for the wavefunctions. The results are

$$C_r = \frac{k_z^A \zeta^A - k_z^B \zeta^B}{k_z^A \zeta^A + k_z^B \zeta^B} \qquad C_t = \frac{2k_z^A}{k_z^A \zeta^A + k_z^B \zeta^B} \tag{5}$$

where $\zeta = f_2 g_{0/}\gamma$, and $k_z = (\gamma - f_1 k_\perp^2) f_2^{-1}$. Note that the incident amplitude of the wavefunction is taken to be unity.

With the help of equation (3) and the probability currents defined by Singh and Wallace (1983), we obtain the probability currents for the incident wave (J_i), reflected wave (J_r), and transmitted wave (J_t) at the interface as follows:

$$\begin{aligned}
J_i &= 2P_\parallel^2(g_1^A + 2g_3^A)k_z^A/(3D_A) \\
J_r &= -J_i C_r^\dagger C_r \\
J_t &= 2P_\parallel^2 C_t^\dagger C_t(g_1^B + 2g_3^B)k_z^B/(3D_B).
\end{aligned} \tag{6}$$

Finally, using the expressions for J_i, J_r, and J_t, we obtain the following expressions for the reflection coefficient (R) and transmission coefficient (T):

$$R = \frac{(k_z^A \zeta^A - k_z^B \zeta^B)^2}{(k_z^A \zeta^A + k_z^B \zeta^B)^2} \qquad T = \frac{4 k_z^A \zeta^A k_z^B \zeta^B}{(k_z^A \zeta^A + k_z^B \zeta^B)^2}. \tag{7}$$

One can easily see that equation (7) satisfies the condition $T + R = 1$ as required by conservation of probability current. Note that due to the in-plane translational invariance, the in-plane wavevector ($\boldsymbol{k}_\perp = (k_x, k_y)$) is the same in both the A and B layers. We have also obtained the expressions for T and R for the case in which an external magnetic field is applied perpendicular to the plane of the interface. The results are given in the appendix.

Now we define the activationless recombination rate per unit energy for electron–hole pairs at the heterointerface as the electron flux crossing from the A layer to the B layer. Note that the recombination processes take place only within the band-overlap region, that is, within the energy interval $E = [0, V_0]$. The expression for the activationless recombination rate per unit energy is written as

$$R_r(E) = \int_0^{k_p} \mathrm{d}k_\perp \; k_\perp \rho_A(E, k_\perp) T_{A\to B}(E, k_\perp) v_z^A(E, k_\perp) \tag{8}$$

where $T_{A\to B}(E, k_\perp)$ is the coefficient of transmission from A to B, $\rho_A(E, k_\perp) = [\partial k_z^A / \partial E]$ is the electron density of states of the A layer, and $v_z^A(E, k_\perp) = [\partial k_z^A / \partial E]^{-1}$ is the velocity of the electron incident from the A layer propagating in the positive z-direction. The upper integration limit for the in-plane wavevector $k_\perp$ in equation (8) is given by $k_p = \min[k_\perp^{A\,max}, k_\perp^{B\,max}]$, where min stands for the minimum value of $k_\perp^{A\,max} = (\gamma_A / f_1^A)^{1/2}$ and $k_\perp^{B\,max} = (\gamma_B / f_1^B)^{1/2}$. By taking the upper bound of the $k_\perp$-integration to be k_p, the condition for electrons crossing the interface without total reflection is automatically taken into account.

Similarly the expression for the activationless generation rate per unit energy is written as

$$R_g(E) = \int_0^{k_p} \mathrm{d}k_\perp \; k_\perp \rho_B(E, k_\perp) T_{B\to A}(E, k_\perp) v_z^B(E, k_\perp) \tag{9}$$

where $T_{B\to A}(E, k_\perp)$ is the coefficient of transmission from B to A, $\rho_B(E, k_\perp) = [\partial k_z^B / \partial E]$ is the electron density of states of the B layer, and $v_z^B(E, k_\perp) = [\partial k_z^B / \partial E]^{-1}$ is the velocity of the electron incident from the B layer propagating in the negative z-direction. When the system is in thermal equilibrium, the generation rate is equal to the recombination rate, i.e., $R_g(E) = R_r(E)$. In other words, in thermal equilibrium, the electron flux due to the generation processes is exactly compensated by the electron flux due to the recombination processes.

Finally, we calculate the current–voltage characteristics of a type II heterojunction. If a voltage is applied to the heterojunction, then the system is no longer in an equilibrium condition, i.e., the Fermi level will no longer be constant throughout the system. As a consequence, there is a net current flow through the interface (Shik *et al* 1998). Hence, the recombination current density crossing the interface from A to B is written as

$$J_{A\to B} = \int_0^{V_0} R_r(E) f_A(E - \mu_A) \left[1 - f_B(E - \mu_B)\right] \mathrm{d}E. \tag{10}$$

Similarly, the generation current density crossing the interface from B to A is given by

$$J_{B\to A} = \int_0^{V_0} R_g(E) f_B(E - \mu_B) \left[1 - f_A(E - \mu_A)\right] \mathrm{d}E \tag{11}$$

where $f_{A,B}(E)$ is the Fermi distribution function and $\mu_{A,B}$ is the Fermi level. Since the generation and recombination processes take place only within the band-overlap region, we must integrate the above expressions over the band-overlap region, i.e., $E = [0, V_0]$. When an external potential (V) is applied, the net current density is written as $J_{net} = J_{A\to B} - J_{B\to A}$ and the external potential satisfies $V = \mu_A - \mu_B$. The conductance per unit area at the interface is simply given by $G = J_{net}/V$.

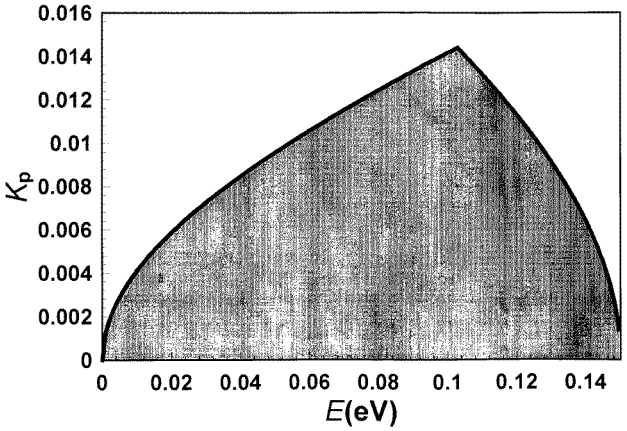

Figure 2. The domain of integration in k_p and E (shaded region) for the generation–recombination current density in an InAs/GaSb heterojunction.

3. Results and discussion

In this section, we present the results of numerical calculations for the activationless recombination rate, and current–voltage characteristics of an InAs/GaSb heterojunction. The band overlap between the conduction band of the InAs semiconductor and the valence band of the GaSb semiconductor is approximately 0.15 eV, and the electrons and the holes are located in the InAs and the GaSb semiconductors, respectively. The following are numerical values for the parameters used in our calculations: $V_0 = 0.15$ eV, $\delta = 0$ eV, $E_{p_\perp} = 22.40$ eV, $E_{p_\parallel} = 22.40$ eV, $E_0^A = 0.42$ eV, $\Delta_A = 0.38$ eV, $E_0^B = 0.81$ eV, and $\Delta_B = 0.755$ eV. In the calculation of the recombination rate and current density one has to calculate the integration limit k_p. In figure 2 we plot the calculated values of k_p as a function of energy E. It is important to note that, when (k_p, $E \leqslant 0.102$ eV) is outside the shaded region in figure 2, k_z^A is imaginary whereas k_z^B is real. On the other hand, when (k_p, $E \geqslant 0.102$ eV) lies outside the shaded region, k_z^A is real while k_z^B is imaginary.

Using equation (8), we can calculate the dimensionless recombination rate $R_r/R_{r(max)}$ as a function of energy E, where $R_{r(max)}$ is the maximum value of the recombination rate R_r. The results are presented in figure 3. The recombination rate $R_r(E)$ vanishes at the band edges, i.e. $E = 0$ and $E = V_0$. This can be easily understood from equation (8), namely the recombination rate $R_r(E)$ is directly proportional to the transmission coefficient $T_{A\to B}(E, k_\perp)$ given by equation (7). The values of the transmission coefficient are zero at the energies $E = 0$ and $E = V_0$, which correspond to the conduction band edge of the InAs semiconductor and the valence band edge of the GaSb semiconductor, respectively. Since there is no band mixing at the band edges, the band overlap between the wavefunction in

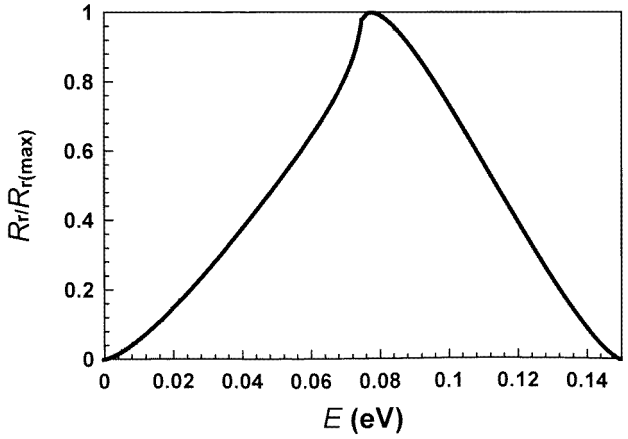

Figure 3. The calculated dimensionless recombination rate $R_r/R_{r(max)}$ as a function of the energy E.

the InAs semiconductor and that in the GaSb semiconductor vanishes at $E = 0$ and $E = V_0$. Hence the recombination rate becomes zero at the end points.

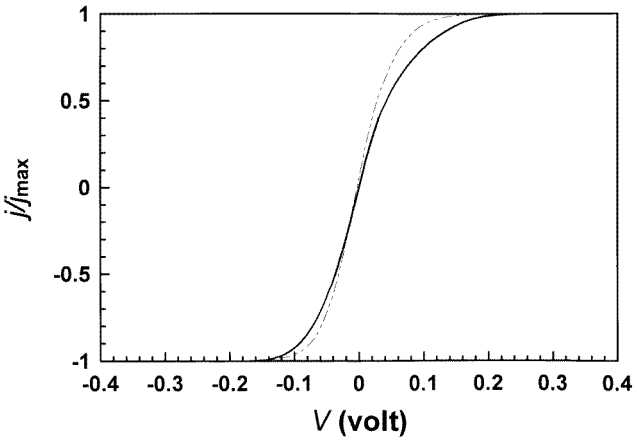

Figure 4. The calculated dimensionless generation–recombination current density J_{net}/J_{max} as a function of applied voltage V at temperature of 100 K (solid line) and 400 K (broken line).

Next we calculate the current–voltage characteristics of an InAs/GaSb heterojunction. We show the calculated dimensionless current density J_{net}/J_{max} as a function of applied voltage V for two different temperatures in figure 4. Here J_{max} is the maximum value of the current density J_{net}. The solid and broken lines correspond to the temperatures 100 K and 400 K, respectively. Under forward bias, i.e. for $V > 0$, the current density J_{net} increases with increasing applied voltage V, becoming non-linear and eventually saturating at a voltage approximately equal to 0.38 V. Note that when the applied voltage is zero, the Fermi level of the InAs semiconductor is the same as that of the GaSb semiconductor. As a result, the net current density J_{net} is zero at $V = 0$ as shown in the figure.

Under reverse bias, i.e. for $V < 0$, the current density also increases with increasing

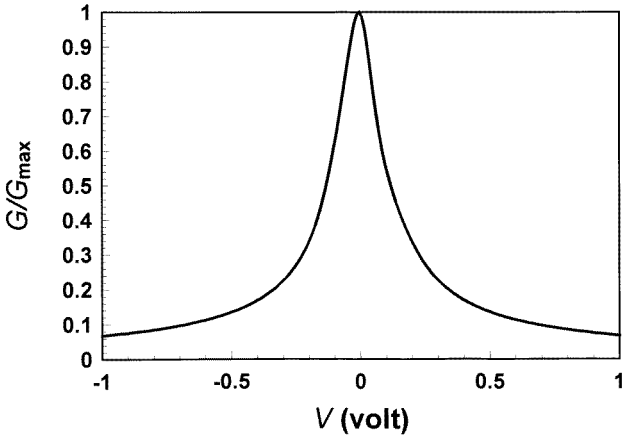

Figure 5. The calculated dimensionless conductance $G/G_{\max}$ as a function of applied voltage V at a temperature of 100 K.

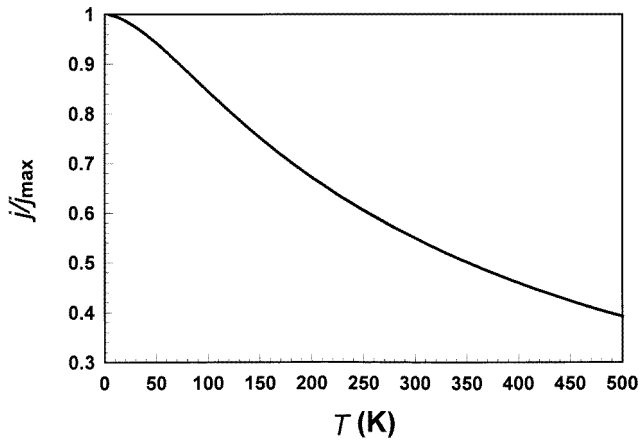

Figure 6. The calculated dimensionless generation–recombination current density $J_{\rm net}/J_{\max}$ as a function of temperature T with applied voltage $V = 0.025$ V.

applied voltage V, becoming non-linear and saturating at a voltage approximately equal to -0.27 V. It is important to note that at small applied voltages, i.e. for $|V| \leqslant 0.02$ V, the current–voltage characteristics are essentially linear. This implies that the InAs/GaSb heterojunction under small applied voltages has the properties of an Ohmic contact, in agreement with the experimental results (Esaki 1980). In addition, we show the calculated dimensionless conductance $G/G_{\max}$ as a function of applied voltage V at a temperature of 100 K in figure 5, where $G_{\max}$ is the maximum value of the conductance G.

Finally, the dimensionless current density $J_{\rm net}/J_{\max}$ as a function of temperature T is shown in figure 6 for a constant applied voltage 0.025 V under forward bias. The figure shows that the current density is inversely proportional to the temperature of the system. As the temperature increases, the number of electrons available for recombination decreases; thus the current density decreases with increasing temperature.

Acknowledgments

The authors are grateful to Professor Alex Shik for helpful discussions. One of the authors (MS) is grateful to NSERC of Canada for financial support in the form of a research grant.

Appendix

In this appendix, we consider the case in which an external magnetic field is applied perpendicularly to the plane of the interface. To take into account heterostructures grown in an arbitrary crystal direction, we define an angle θ between the growth axis and the c-axis corresponding to the [001] crystal direction (Singh and Wallace 1983). The energy dispersion relation within each layer is written as

$$\gamma(E_n) = \frac{2n+1}{l^2}\sqrt{f_1 A_1} + f_1 f_2^{-1} A_1 k_z^2 \pm \frac{P_\perp \Delta}{3l^2} A_3$$

where

$$A_1 = f_1 \sin^2[\theta] + f_2 \cos^2[\theta]$$
$$A_2 = (f_1 - f_2)\sin[\theta]\cos[\theta]$$
$$A_3 = [P_\perp^2 (E_n + E_0 + \delta)^2 \cos^2[\theta] + P_\parallel^2 (E_n + E_0)^2 \sin^2[\theta]]^{-1}$$

and l is the usual cyclotron radius, and n is the Landau quantum number.

Following the same method as described in the theory section, we found the values of the reflected and transmitted amplitudes: $C_\mathrm{r} = C_+/C_-$ and $C_\mathrm{t} = C/C_-$, where

$$C = 2\lambda k_z^\mathrm{A} \zeta_1^\mathrm{A} (\alpha_\mathrm{A}^\dagger \alpha_\mathrm{A} + \beta_\mathrm{A}^\dagger \beta_\mathrm{A})$$
$$\begin{aligned} C_\pm = {} & (k_z^\mathrm{A} \zeta_1^\mathrm{A} \alpha_\mathrm{A}^\dagger \alpha_\mathrm{A} \pm \zeta_2^\mathrm{A} \alpha_\mathrm{A}^\dagger \alpha_\mathrm{A} \pm \zeta_3^\mathrm{A} \alpha_\mathrm{A}^\dagger \beta_\mathrm{A} + k_z^\mathrm{A} \zeta_1^\mathrm{A} \beta_\mathrm{A}^\dagger \beta_\mathrm{A} \pm \zeta_2^\mathrm{A} \beta_\mathrm{A}^\dagger \beta_\mathrm{A} \pm \zeta_3^\mathrm{A} \beta_\mathrm{A}^\dagger \alpha_\mathrm{A}) \\ & \mp \lambda (k_z^\mathrm{B} \zeta_1^\mathrm{B} \alpha_\mathrm{A}^\dagger \alpha_\mathrm{B} + \zeta_2^\mathrm{B} \alpha_\mathrm{A}^\dagger \alpha_\mathrm{B} + \zeta_3^\mathrm{B} \alpha_\mathrm{A}^\dagger \beta_\mathrm{B} + k_z^\mathrm{B} \zeta_1^\mathrm{B} \beta_\mathrm{A}^\dagger \beta_\mathrm{B} \\ & + (\zeta_2^\mathrm{B})^\dagger \beta_\mathrm{A}^\dagger \beta_\mathrm{B} + (\zeta_3^\mathrm{B})^\dagger \beta_\mathrm{A}^\dagger \alpha_\mathrm{B}) \end{aligned}$$

with

$$\lambda = (\alpha_\mathrm{A}^\dagger \alpha_\mathrm{B} + \beta_\mathrm{A}^\dagger \beta_\mathrm{B})^{-1} \qquad \alpha = \sin[\tau_\mathrm{n}] \qquad \beta = \cos[\tau_\mathrm{n}]$$
$$\tau_\mathrm{n} = \tan^{-1}[\tan[\theta P_\parallel g_1 / P_\perp g_7]]$$
$$\zeta_1 = (f_1 \sin^2[\theta] + f_2 \cos^2[\theta]) g_0 \gamma^{-1}$$
$$\zeta_2 = [(f_1 - f_2) g_0 \gamma^{-1} \sin[\theta]\cos[\theta] + \mathrm{i}\, 3 P_\perp^2 g_0 g_6 g_7 \gamma^{-1} \sin[\theta]][2n+1]$$
$$\zeta_3 = P_\parallel P_\perp g_0 g_1 g_6 [(\cos^2[\theta] + \sqrt{2}\sin^2[\theta]) + \mathrm{i}\cos[\theta]](2n+1)/(\sqrt{2}\gamma).$$

The transmission and reflection coefficients are given by $T = J_\mathrm{t}/J_\mathrm{i}$ and $R = J_\mathrm{r}/J_\mathrm{i}$, respectively. Here $J_\mathrm{t} = J_+^\mathrm{B} C_\mathrm{t}^\dagger C_\mathrm{t}$, $J_\mathrm{r} = J_-^\mathrm{A} C_\mathrm{r}^\dagger C_\mathrm{r}$, and $J_\mathrm{i} = J_+^\mathrm{A}$, where

$$\begin{aligned} J_\pm = \Bigg[& \frac{1}{2}(P_\perp^2/g_1)(\sin[\theta] \pm h\cos[\theta])\sin[\theta] \pm \frac{2}{3}(P_\parallel^2 g_3/D)(\cos[\theta] \mp h\sin[\theta])\cos[\theta] \\ & + \frac{1}{6}(P_\perp^2 g_8/D)(\sin[\theta] \pm h\cos[\theta])\sin[\theta] \\ & \pm \frac{1}{3}(P_\parallel^2 g_1/D)(\cos[\theta] \mp h\sin[\theta])\cos[\theta] \\ & + \frac{1}{3}(P_\perp^2 g_7/D)(\sin[\theta] \pm h\cos[\theta])\sin[\theta]][k_z \alpha^\dagger \alpha + k_z \beta^\dagger \beta] \end{aligned}$$

$$+\frac{1}{3}(P_{\|}P_{\perp}/D)[k_z\alpha^{\dagger}\beta + k_z\beta^{\dagger}\alpha][(g_8 - g_7)(\sin[\theta] \pm h\cos[\theta])\sin[\theta]$$
$$\pm (g_1 - g_3)(\cos[\theta] \mp h\sin[\theta])\cos[\theta]\Big] + \text{CC}$$

with

$$h = (f_2 - f_1)\sin[\theta]\cos[\theta]/(f_2\cos^2[\theta] - f_1\sin^2[\theta])$$

and where CC stands for the complex conjugate.

The recombination rate per unit energy is given by

$$R_{\text{r}}(E_n) = \frac{1}{4\pi^2}\sum_{n=0}^{N_{\min}}\sqrt{(2n+1)l^{-1}}\rho_{\text{A}}(E_n)T_{\text{A}\to\text{B}}(E_n)v_z^{\text{A}}(E_n)$$

where $N_{\min}$ is defined as $N_{\min} = \min[n_{\max}^{\text{A}}, n_{\max}^{\text{B}}]$. The expression for $n_{\max}$ is obtained from the dispersion relation and is written as

$$n_{\max} = \text{Round}\left[\frac{1}{2}[(l^2\gamma \mp P_{\perp}\Delta A_3/3)(f_1 A)^{-1/2} - 1]\right]$$

where Round[ ] indicates rounding the argument to the nearest non-negative integer. Finally using $R_{\text{r}}(E_n)$ together with equation (10), one can calculate the current density for the heterojunction in the presence of an external magnetic field.

References

Barnes D J, Nicholas R J, Mason N J, Walker P J, Warburton R J and Miura N 1993 *Physica* B **184** 168 and references therein

Bastard G 1988 *Wave Mechanics Applied to Semiconductor Heterostructures* (Paris: Les Editions de Physique)

Bastard G, Brum J A and Ferreira R 1991 *Solid State Physics, Semiconductor Heterostructures and Nanostructures* vol 44, ed H Ehrenreich and D Turnbull (New York: Acadamic)

Bodnar J 1978 *Narrow Gap Semiconductors, Physics and Applications; Proc. Int. Summer School* (Warsaw: Polish Scientific)

Esaki L 1980 *Narrow Gap Semiconductors, Physics and Applications; Proc. Int. Summer School* (Berlin: Springer)

Kono J and McCombe B D 1997 *Phys. Rev.* B **55** 1617 and references therein

Lamrani H E A and Aubin M J 1987 *J. Phys. C: Solid State Phys.* **65** 199 and references therein

Lau W and Singh M 1996a *Phys. Status Solidi* b **193** 269

——1996b *Solid State Commun.* **100** 359 and references therein

Sakaki H, Chang L L, Ludeke R, Chang C A, Sai-Halasz G A and Esaki L 1977 *Appl. Phys. Lett.* **31** 211

Seiler D G, Bajaj B D and Stephens A E 1977 *Phys. Rev.* **161** 2882 and references therein

Shik A, Singh M and Lau W 1998 private communication

Singh M and Wallace P R 1983 *J. Phys. C: Solid State Phys.* **16** 3877

Wallace P R 1979 *Phys. Status Solidi* b **92** 49